0550

N65-29172

FACILITY FORM 602

(ACCESSION NUMBER)	(THRU) 1
42 (PAGES)	(CODE)
CR 63894 (NASA CR OR TMX OR AD NUMBER)	14 (CATEGORY)

QUARTERLY PROGRESS REPORT NO. 2

CONTRACT NO. NASw-1035

HUGHES

HUGHES AIRCRAFT COMPANY

HUGHES RESEARCH LABORATORIES • MALIBU

GPO PRICE $ _____

CFSTI PRICE(S) $ _____

Hard copy (HC) 2.00

Microfiche (MF) .50

ff 653 July 65

HUGHES RESEARCH LABORATORIES
Malibu, California

a division of hughes aircraft company

RESEARCH ON GRAVITATIONAL MASS SENSORS

Quarterly Progress Report No. 2
Contract No. NASw-1035
15 January through 14 April 1965

Robert L. Forward, Principal Investigator
Curtis C. Bell and J. Roger Morris,
Contributors

TABLE OF CONTENTS

	LIST OF ILLUSTRATIONS		v
I.	INTRODUCTION AND SUMMARY		1
	A.	Purpose and Technical Objectives	1
	B.	Summary of Problem Areas	1
	C.	Summary of General Approach	2
	D.	Summary of Work to Date	2
II.	EXPERIMENTAL PROGRAM		7
	A.	Phase Shift Tuned Amplifier	7
	B.	Cruciform Vibrational Mode Behavior	12
	C.	Air Bearing Drive and Support	22
III.	THEORETICAL PROGRAM		27
	A.	Air Bearing Analysis	27
	B.	Cruciform Sensor Analysis	32
IV.	CONCLUSIONS		39
V.	RECOMMENDATIONS		41

LIST OF ILLUSTRATIONS

Fig. 1.	Generalized phase shift tuned amplifier	7
Fig. 2.	Optimized phase shift tuned amplifier	9
Fig. 3.	Equivalent LC circuit	10
Fig. 4(a).	Solid Mount	15
Fig. 4(b).	Torsion Mount	16
Fig. 5(a).	Sensor cruciform (2 in. radius)	19
Fig. 5(b).	Sensor cruciform (1 in. radius)	20
Fig. 5(c).	Sensor cruciform (1/4 in. radius)	21
Fig. 6.	Air bearing support and drive (assembled)	23
Fig. 7.	Air bearing support and drive (exploded view)	24
Fig. 8.	Air bearing table schematic	28
Fig. 9.	Cruciform analysis schematic	33

I. INTRODUCTION AND SUMMARY

A. Purpose and Technical Objectives

The ultimate objective of our effort on gravitational mass sensors is the development of a small, lightweight, rugged sensor to be used on lunar orbiters to measure the mass distribution of the moon and on deep space probes to measure the mass of the asteroids. The basic concepts, the theoretical limitations, and the possible applications have been investigated and are discussed in Section II of Quarterly Progress Report No. 1.

The purpose of the present research program is

1. To develop and refine experimental techniques for the measurement of gravitational and inertial fields, using rotating elastic systems.

2. To develop a more complete understanding of these types of sensors so that accurate predictions of sensor behavior can be made which are based on practical system configurations and measured device sensitivity.

B. Summary of Problem Areas

The major problem area can be summarized in one word — noise. This noise includes background clutter due to external forces and masses other than the one under investigation, external electrical noise and mechanical vibrations, and internal thermal and electronic noise in the sensor and amplifiers. The force of gravitational attraction is very weak, even for large masses, and every effort must be made in sensor design and operation to develop and utilize discrimination techniques that will allow the weak gravitational signal to be picked out from the background clutter and noise.

The problems of background clutter are nearly independent of the particular sensor design. It is felt that the techniques discussed in Section II-D-2 of Quarterly Progress Report No. 1, Background Rejection, will suffice for elimination of this source of noise.

The problems of externally and internally generated electrical and mechanical noise have been overcome in previous work on non-rotating gravitational sensors and the experience gained during this work will aid in the investigation of the very similar problems in rotating sensors. It is expected that each sensor design will have its own versions of these problems and that a major portion of the experimental work will be spent in locating and eliminating or discriminating against these sources of extraneous noise.

One minor problem area which will require special attention in the theoretical portion of the program is the instability and cross-coupling effects that are common to mechanically rotated systems. Typical examples are given in the Appendix of Quarterly Progress Report No. 1. These problems can be avoided by proper choice of sensor configuration and sensor operation based on a thorough theoretical analysis and preliminary experimental studies of each proposed design before extensive experimental work is done.

C. Summary of General Approach

The program has started with parallel efforts consisting of detailed theoretical study and preliminary experimental work. The various possible sensor configurations are being investigated theoretically to determine their suitability as mass sensors under the assumed operating conditions. Various combinations of promising sensor designs and sensor support and drive mechanisms are being constructed and will be operated to verify qualitatively the sensor characteristics, develop signal readout techniques, and search for unexpected sources of instabilities and noise. No attempt will be made to look for gravitational interactions at this stage.

After the preliminary work, one of the sensor configurations will be chosen as the basis for a feasibility model, and a carefully designed version will be constructed. The remainder of the program will be expended in studying the feasibility model both experimentally and theoretically, locating and eliminating the sources of extraneous noise, and determining the sensitivity to gravitational fields. The program objective is a sensor that will detect the presence of a small, nearby moving mass through gravitational interactions.

D. Summary of Work to Date

This work began when the completed contract was received on 26 October 1964. The original study by R. L. Forward on the gravitational mass sensor[1] was analyzed by C. C. Bell in a more general manner. (See Appendix of Quarterly Progress Report No. 1.) This analysis indicates that radially vibrating sensor structures generally are incapable of measuring the gravitational force gradient because the sensor will fly apart at the necessary rotation speeds.

A theoretical study of a transversely vibrating cruciform sensor structure which does not have this instability problem has been started by C. C. Bell. The model used for the analysis consists of a central mass, four equal sensing masses on transversely vibrating arms, and a sensed mass. The preliminary solution yielded the following expression for the maximum voltage output V of the sensor due to the presence of a mass M at a distance R,

$$V = \frac{3GM}{8R^3} \frac{\tau}{\omega} \frac{hr}{L^2} \sigma \sin 2\omega t$$

where

$GM/R^3 \equiv$ gravitational gradient

$\omega \equiv$ angular frequency or rotation of the sensor

$\tau \equiv$ integration time

$r \equiv$ radial distance of sensor end mass from center of sensor rotation

$L \equiv$ length of sensor arm

$h \equiv$ thickness of sensor arm

$\sigma \equiv$ transducer factor of strain transducer (V/in./in.)

It was assumed that the rotation speed of the sensor was constant at ω, that the center of mass of the sensor did not translate in space, and that there was no elastic coupling between the arms of the sensors.

The output for the cruciform sensor predicted by the above equation is lower than the output of a similar sized radial spring sensor by a factor of hr/L^2 (see eq. (19) of Quarterly Progress Report No. 1). In the current design this factor is about 0.07. Other sensor designs which will increase the voltage output by varying the parameters h, r, and L are being considered.

The above simplified solution is adequate for an order of magnitude estimate of the output of the sensor, but it neglects the interaction between the arms. A more detailed analysis of these sensors is in progress.

A cruciform sensor head (with associated vacuum chamber), designed by C. C. Bell, was built for test purposes. The sensor head has four arms which vibrate tangentially to the direction of rotation. The arms are about 1.5 in. long, 0.75 in. wide, and 0.050 in. thick; each has a 0.75 in. cube at its end for extra mass. The sensor has a resonance at 190 cps with a Q of 170 in air. The four strain transducers, one on each arm, have a voltage-strain characteristic of 3.5×10^5 V/unit strain. The associated vacuum chamber, which will be rotated with the sensor head, is 5.5 in. in diameter and 1.5 in. thick.

Readout from the rotating sensor chamber is accomplished with standard slip rings. J. R. Morris has designed an alternative method of readout which involves inductive coupling between a static coil and a rotating coil containing a ferrite rod.

A detailed theoretical and experimental study of a phase shift tuned amplifier was carried out by Morris (see Section II-A). The phase shift tuned amplifier is identical to the familiar phase shift oscillator except that it has an input and its gain is reduced to slightly below that required for oscillation. The gain need be no larger than 8 in order to obtain any desired Q.

This circuit is valuable for our application because the series capacitance of the strain transducer used to sense the vibrations becomes part of the tuned amplifier. The result is identical to tuning the gauge with a very large inductor (approximately 500 h).

The experimental work showed high effective gain (150 for one transistor) and strong coupling between mechanical and electrical resonant circuits.

This circuit will be useful as a first preamplifier stage provided that the fine tuning may be satisfactorily accomplished by varying the supply voltage.

Morris has also developed a standard preamplifier circuit using two field effect transistors and one ordinary transistor (a total of 16 components) for boosting the strain transducer output. The circuit has a gain of 120, an input impedance of 2.5 MΩ, and an equivalent input noise of less than 0.2 μV in a 5% pass band at 190 cps.

The sensor (in its vacuum chamber) was placed in a ball bearing support frame and driven to a rotational speed of 6000 rpm (100 cps) to check the gross characteristics of the sensor in a rotating system and to study readout techniques. The slip rings worked quite well at these speeds and the only effect of the rotation on the sensor seemed to be a shift in the resonance frequency from 190 to 200 cps. This initial test demonstrated the basic structural stability of the cruciform design while under rotation. As expected, the vibrational noise from the mechanical bearings was too great (20 mV) to permit observation of gravitational interactions with this unit.

An air bearing support and drive was constructed for this program by the Hughes Aerospace Group. The structure consists of a table supported both vertically and horizontally by an air bearing formed with a rotor tube sitting on a channeled stator. The rotor tube also has a magnetic hysteresis ring which is excited and driven by a synchronous motor stator constructed around the outside (see Section II-C). The

sensor chamber is then mounted on top of the rotor table and the voltages from the sensor are removed through the slip rings on the top. This support and drive unit was constructed primarily for discovery and investigation of vibrational noise sources in air bearings.

The air bearing has very low friction, but two noise sources were discovered. One was a lateral dynamic resonance which would occur at speeds just short of the desired rotational speeds when the rotor table was loaded with the sensor chamber. The other was a vertical instability, which would occur even with a stationary, but levitated, table. The noise level introduced into the sensor by these vibrations was large enough to cause a sensor output in the millivolt range. A theoretical analysis (Section III-A) indicated the possible causes of this instability and the air bearing portion of the unit is being modified in an attempt to eliminate the problem.

A Beams type magnetic suspension and drive is being fabricated by W.H. Dancy of the University of Virginia. Delivery is expected 1 June 1965.

Quartz strain transducers have been ordered from the Valpey Corporation. They have less output and higher impedance than the barium titanate transducers, but are intrinsically more stable and have a higher mechanical Q.

When the cruciform sensor head was mounted in its vacuum chamber on a stiff supporting rod, it was found that three vibrational resonant modes were present instead of one, as expected. The two extra modes were thought to be caused by the sensor modes coupling to the mass of the vacuum chamber through the support rod. To check this possibility, the sensor was removed from the solid mount and suspended alone from its center by a wire and a rubber strip. The four primary piezoelectric strain transducers were then driven with a constant voltage and the sensor response detected with a fifth transducer. By applying properly phased driving voltages to the transducers on the various arms, it was possible to excite the various modes selectively.

The gradient or tuning fork mode is at 189 cps and the angular acceleration or rotational mode is at 993 cps. The transitional acceleration or wing flapping mode was found to split into two modes at 241 and 244 cps because of the slight dimensional differences between the opposite pairs of arms.

A small mass weighing approximately 10 g was then added to the center mass of the cruciform, and the measurements repeated. It was found that the tuning fork mode remained the same, the translation modes each shifted downward about 10 cps, and the torsional mode shifted from 993 to 977 cps. Further increases in the central mass caused the translational and tuning fork modes to overlap.

Because of the shifting mode problems experienced with a solid mount, a softer mount consisting of a torsion wire connected to the top and bottom of the vacuum chamber was designed. Tests on the first model of this suspension have shown favorable results. The sensor modes remain well separated from each other and it is possible to filter out the contributions of all the other modes of sensor vibration from the desired gradient or tuning fork mode. The vibrational coupling of the torsion mount is also less by an order of magnitude than that of the solid mount used previously.

A new chamber design for this type suspension has been completed and is now being fabricated. The new design will feature greater versatility of the chamber to adapt to various types of torsion bar configurations, tighter tolerances to alleviate balance problems, a more reliable means of evacuating and leak testing the rotor assembly, and other changes which will facilitate assembly of the cruciform, torsion bar, rotor, and chamber. A new rotor evacuation fixture has also been designed and is ready for fabrication. This fixture will be readily adaptable to all foreseeable rotor configurations.

Tests were made on a set of three cruciform sensors which had the same arm length and end mass but different radii of curvature between the arms in order that the effect of the radius of curvature on the sensor frequency and Q could be determined (Section II-B). The frequency of the three sensors in the tuning fork mode were the same although their over-all diameters were considerably different due to the different radii of curvature. The sensor with the smallest radius of curvature had the greatest separation between the various vibrational modes because of its smaller center mass. The effect on the Q of the sensors was negligible in comparison with the unavoidable lowering of the Q from the attachment of the strain transducers.

II. EXPERIMENTAL PROGRAM

A. Phase Shift Tuned Amplifier

The mechanical vibrations of interest on this program are detected by means of piezoelectric strain transducers. The transducers used have a high voltage output (> 10^5 V/unit strain), but they also have a characteristic small series output capacity (typically 1000 pF).

Because the vibrations of interest are extremely small, and signal-to-noise problems are of paramount importance, it is desirable to tune out the capacity rather than work into high impedance. The low capacity value and low frequencies of interest (typically 200 cps) preclude the use of an inductor, however. A small, simple circuit which behaves like an inductor is needed. The phase shift tuned amplifier fulfills these requirements.

Figure 1 shows the amplifier circuit. It is identical to the conventional phase shift oscillator circuit except that it has an input, and its gain is adjusted so that it is not quite sufficient for oscillation.

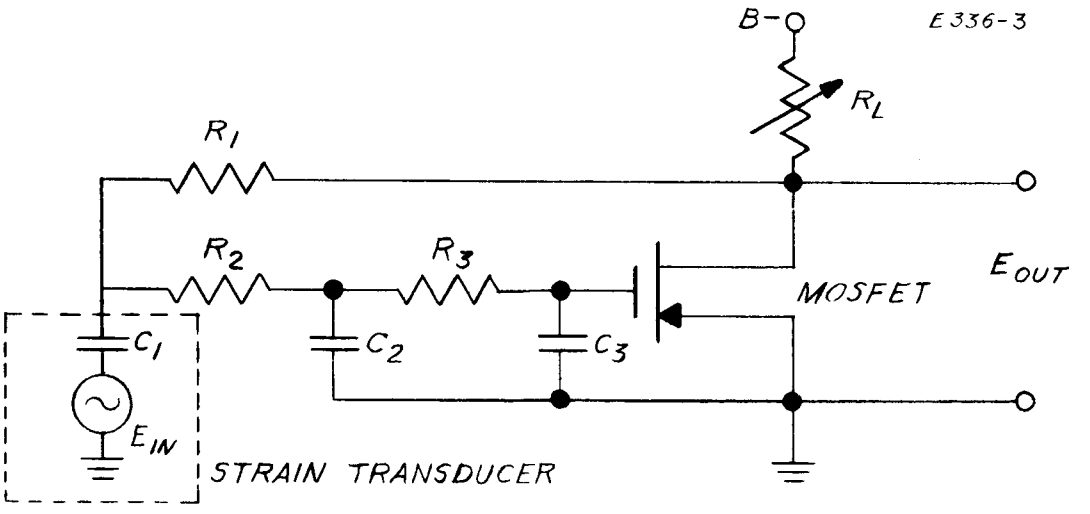

Fig. 1. Generalized phase shift tuned amplifier.

The MOSFET (Metal Oxide Silicon Field Effect Transistor) is ideal for this circuit since it has essentially infinite input resistance ($>10^{15}\ \Omega$) and operates with a forward bias equal to its drain (collector) voltage.

The complete relationship between input and output is:

$$\frac{E_{out}}{E_{in}} = \frac{-AsC_1R_1}{s^3C_1C_2C_3R_1R_2R_3 + s^2(C_1C_2R_1R_2 + C_2C_3R_2R_3 + C_1C_3R_1R_3 + C_2C_3R_1R_3 + C_1C_3R_1R_2) + s(C_1R_1 + C_2R_2 + C_3R_3 + C_2R_1 + C_3R_1 + C_3R_2) + A + 1} \qquad (1)$$

where $s = j\omega$ and A is the gain of the MOSFET transistor.

This equation is considerably simplified if we let $R_1 = R$, $R_2 = NR$, $R_3 = N^2R$, and $C_1 = C$, $C_2 = C/N$, $C_3 = C/N^2$.

Then,

$$\frac{E_{out}}{E_{in}} = \frac{-AsCR}{(sCR)^3 + [3 + (2/N)]\,(sCR)^2 + [3 + (2/N) + (1/N^2)]\,(sCR) + A + 1} \qquad (2)$$

(See Fig. 2.)

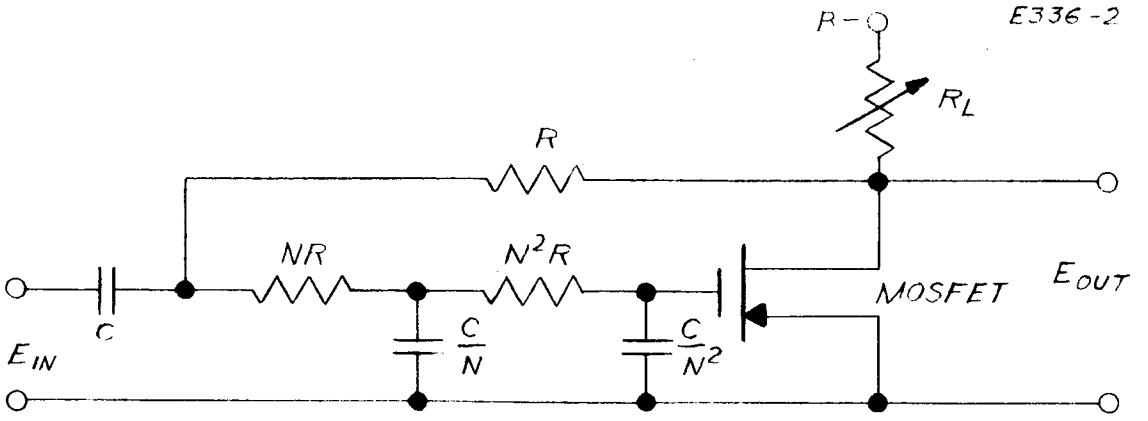

Fig. 2. Optimized phase shift tuned amplifier.

For this circuit, resonance will occur at

$$\omega = \frac{\sqrt{3 + (2/N) + (1/N^2)}}{CR} \tag{3}$$

when the MOSFET transistor gain is adjusted to:

$$A = 8 + \frac{12}{N} + \frac{7}{N^2} + \frac{2}{N^3} \quad . \tag{4}$$

Although the resonance denominator of eq. (2) is fairly complicated, the calculated and observed resonance of the circuit for high N and high gain consists of a simple resonance shape that is almost indistinguishable from a typical LC resonance curve of the same amplitude and Q.

In order to develop expressions for an equivalent resonance frequency and Q for the phase shift tuned amplifier, we will let N be very large; then

$$\frac{E_{out}}{E_{in}} = \frac{-AsCR}{(sCR+1)^3 + A} \quad . \tag{5}$$

This relationship may be rearranged as follows:

$$\frac{E_{out}}{E_{in}} = \frac{AQ}{\left[j\frac{\omega}{\omega_o}\left(1 - A^{1/3} + A^{2/3}\right)^{1/2} + 1 + A^{1/3}\right]\left[1 - A^{1/3} + A^{2/3}\right]^{1/2}}$$

$$\div \left[1 + jQ\left(\frac{\omega_o}{\omega} - \frac{\omega}{\omega_o}\right)\right] \tag{6}$$

where

$$Q = \frac{\left(1 - A^{1/3} + A^{2/3}\right)^{1/2}}{2 - A^{1/3}} \tag{7}$$

$$\omega_o = \frac{\left(1 - A^{1/3} + A^{2/3}\right)^{1/2}}{RC} \quad . \tag{8}$$

Note that the Q of the circuit resonance becomes very large as the gain of the MOSFET transistor A approaches 8. For gains higher than 8 the amplifier becomes an oscillator. Since we will normally be operating at high Q's, we can assume that $A \cong 8$, and the above equations become

$$Q \cong \frac{\sqrt{3}}{2 - A^{1/3}} \tag{9}$$

$$\omega_o \cong \frac{\sqrt{3}}{RC} \tag{10}$$

Note that for high Q, the slight dependence of the resonant frequency ω_o on the gain disappears.

At resonance, where $\omega = \omega_o$ and for a Q greater than 25, the circuit gain (eq. (6)) and the input impedance simplify to

$$\frac{E_{out}}{E_{in}} \cong 1\frac{1}{3}\, Q \angle 150^\circ \tag{11}$$

$$Z_{in} \cong \frac{R\sqrt{3}}{2Q} \angle 0^\circ \tag{12}$$

These circuit parameters are to be compared with the equivalent LC circuit parameters (see Fig. 3), which are

$$Q = \frac{\omega_o L}{R_L} \tag{13}$$

$$\omega_o = \frac{1}{\sqrt{LC}} \tag{14}$$

$$\frac{E_{out}}{E_{in}} \cong Q \angle 90^\circ \tag{15}$$

$$Z_{in} = R_L \angle 0^\circ \quad . \tag{16}$$

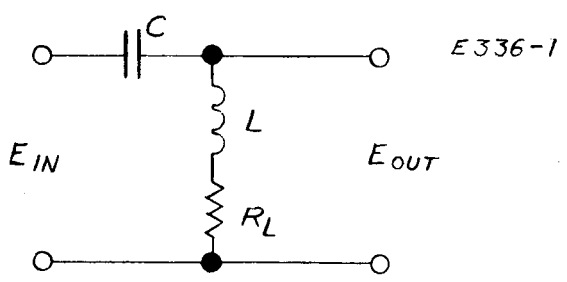

Fig. 3. Equivalent LC circuit.

The input capacitance C is the capacitance of the strain transducer.

Although the circuit has been analyzed for the ideal case, the formulae describe the general circuit behavior and are useful for high values of N. The circuit will work for any value of N, but if N is small, the gain necessary for a high Q may be more than the MOSFET can deliver.

Because of the high input resistance of MOSFET's, the value of R_3 is limited only by the MOSFET input capacity (typically 8 pF).

To verify the analytical study experimentally, a circuit with variable resistors was connected to a cruciform mass sensor. One strain transducer was used as a control. Another transducer was connected alternately to the tuned amplifier circuit and to an oscilloscope. The mechanical resonant frequency of the sensor was found by exciting the sensor acoustically and peaking the monitor transducer output. The output transducer indicated 1 mV peak-to-peak on the oscilloscope at resonance.

The output transducer was then coupled into the test circuit. The gain and RC time constants were adjusted to reduce the monitor transducer output by 3 dB. Since the acoustic excitation was not changed, this indicates that a significant portion of the stored vibrational energy was being extracted from the sensor. The output of the test circuit was measured to be 150 mV.

The experiment showed high effective gain (150 for one transistor) and strong coupling between mechanical and electrical resonant circuits.

This circuit will be useful as a first preamplifier stage provided that the fine tuning may be satisfactorily accomplished by varying the supply voltage. Since no previous record of its use has been found, a patent disclosure has been filed.

B. Cruciform Vibrational Mode Behavior

A cruciform sensor head, which was designed by C. C. Bell, was fabricated during the last quarter; it was described in Section III-A of the first quarterly report. When the sensor head was mounted in a vacuum chamber on a stiff supporting rod, it was found that three vibrational resonant modes were present (e.g., 186.2, 187.7, and 190.1 cps) instead of one, as expected. The coupling of the sensor modes to the mass of the vacuum chamber through the support rod was believed to be the cause. To check this possibility, the sensor was removed from the solid mount and suspended alone from its center by a wire and a rubber strip. The four primary piezoelectric strain transducers were then driven with a constant voltage and the sensor

response detected with a fifth transducer. By applying properly phased driving voltages to the transducers on the various arms, it was possible to excite the various modes selectively. The results are shown in Table I.

This table shows that the various modes are all well separated from each other if the center of the sensor is not strongly coupled to a large mass. It was possible to identify the primary modes of interest from the large responses at particular modes for particular driving phase combinations. The gradient or tuning fork mode is at 189 cps and the angular acceleration or rotational mode is at 993 cps. The transitional acceleration or wing flapping mode was found to split into two modes at 241 and 244 cps because of the slight dimensional differences between the opposite pairs of arms. The other modes were not directly identified, but could easily be torsional modes as well as harmonics of the above vibrational modes since the transducers were not placed exactly along the central line of the arms on this sensor.

A small mass (approximately 10 g) was then added to the center mass of the cruciform, and the measurements repeated. It was found that the tuning fork mode remained the same, the translational modes each shifted downward about 10 cps, and the torsional mode shifted from 993 to 977 cps.

The results of these measurements indicated that the desired mode of operation (the tuning fork or gradient mode) has the lowest frequency of vibration and its output can be well separated from all the other vibrational modes by a simple band-pass filter if the sensor's effective central mass can be kept small. This indicated that further effort was needed on the sensor support mechanism as well as on the sensor design.

1. Torsion Mount

A soft mount consisting of a torsion wire (0.014 in. steel) connected to the top and bottom of the vacuum chamber was designed, because of the shifting mode problems experienced with the solid mount. Although it had the desired minimum amount of coupling between the sensor and the chamber, this first model was too weak to take the imbalances experienced at high rotations with the present sensor designs. The new sensor designs will be adjustable and the dynamic balancing improved to the point where the torsion wire will be able to stand the centrifugal forces.

In order to compare the merits of the solid suspension and the torsion suspension, two chambers were assembled and tested on the air bearing table. (See Fig. 4.)

TABLE I

Driven Resonant Modes

Tuning Fork Mode		Torsional Mode		Translational Mode	
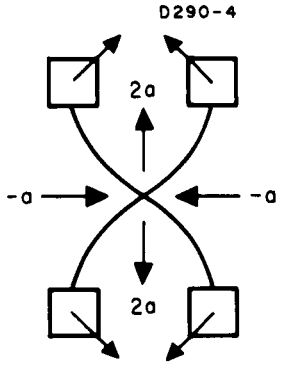		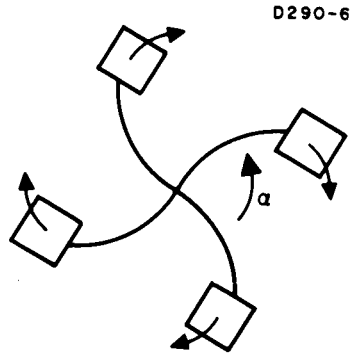		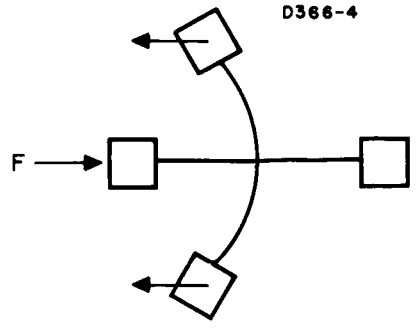	
Frequency cps	Output mV	Frequency cps	Output mV	Frequency cps	Output mV
189.0	37	188.8	11.2	188.8	2
243.8	6	244.3	4.2	241 244.4	27
845.5	6.5	849.5	5.7	845.5	7
869.0	2.5	869.0	<1	869.0	1
992.9	13	993.0	58	993.0	4.5
1745	40	1745	52	1745	33
1989	16	1949	7	1949	8.8
2048	17	2084	22	2039 2084	1.5 9

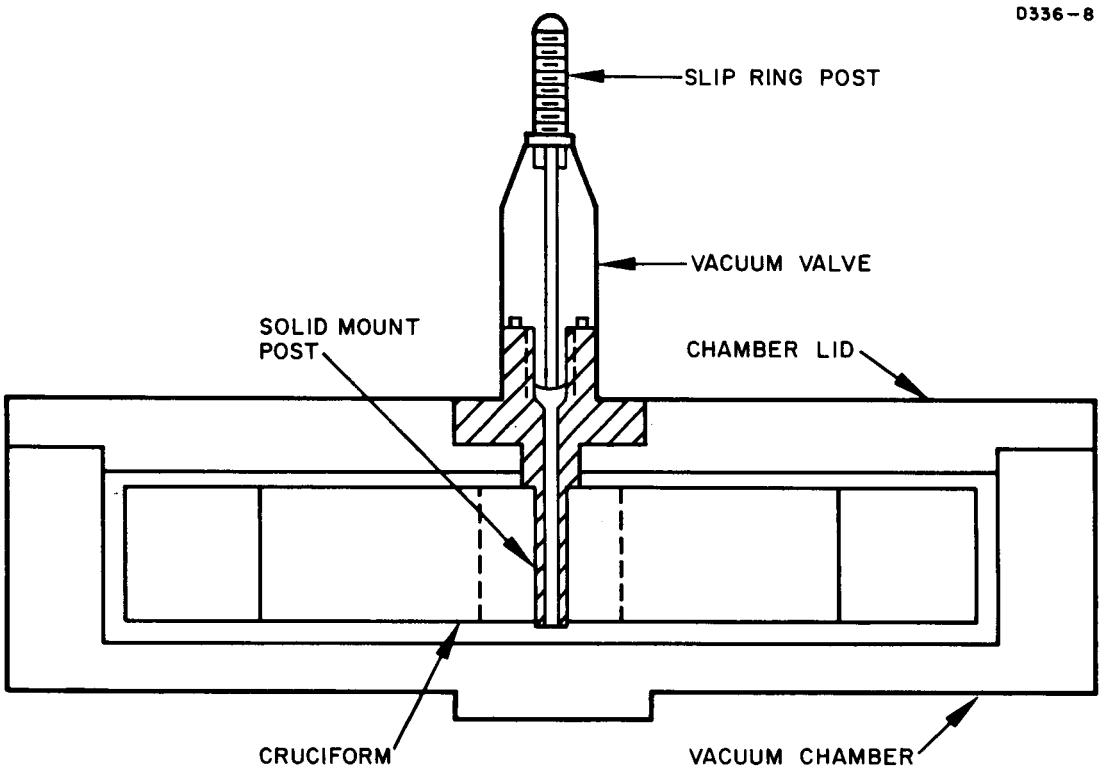

Fig. 4(a). Solid mount.

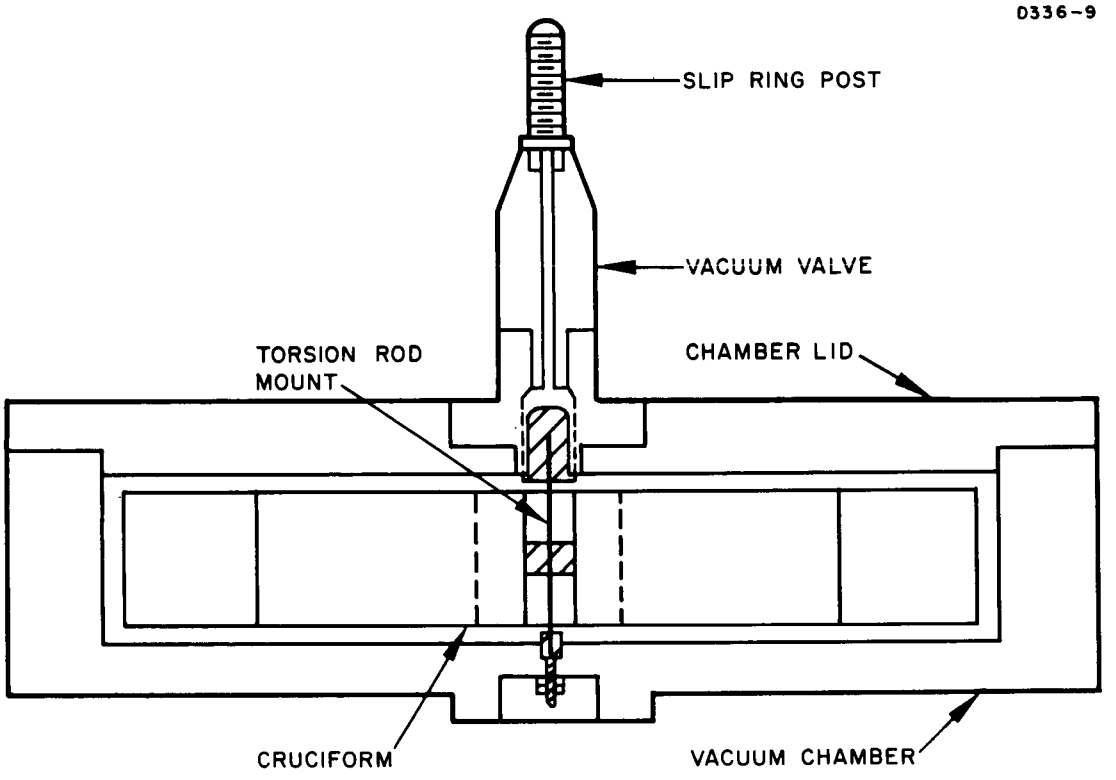

Fig. 4(b). Torsion mount.

Both sensors gave outputs of a few hundred microvolts at rotation speeds not related to their resonant frequencies. They were compared at one quarter of the desired rotation speed, and the torsion mount response to the noise at these frequencies was an order of magnitude better than the solid mount. (See Table II.)

TABLE II

Comparison of Solid Mount and Torsion Mount

Unit	Vibrational Frequency, cps	Test Rotation Speed, rpm	Output, mV
Solid Mount (Fig. 4(a))	172	1290	25
Torsion Mount (Fig. 4(b))	192	1440	2

Both mounts were also tested by evacuating their chambers, exciting the chamber acoustically at the resonant frequency of the sensor, and reading the response of the sensors to the noise passed by the supports. Again the output of the sensor with the torsion mount was an order of magnitude less.

A new chamber design for this type of suspension has been completed and is being fabricated. The new design will feature greater versatility of the chamber to adapt to various types of torsion mount configurations, tighter tolerances to alleviate balance problems, a more reliable means of evacuating and leak testing the rotor assembly, and other changes which will facilitate assembly of the cruciform, torsion mount, and chamber. A new rotor evacuation fixture has also been designed and is ready for fabrication. This fixture will be readily adaptable to all foreseeable rotor configurations.

2. Multiple Radius Tests

Since an increase in the center mass of the cruciform has a tendency to converge the frequencies of the various vibrational modes, it is desirable to keep the center mass as small as possible by making as small as possible the radii of curvature of the fillets between the arms. The original purpose of this fillet was to prevent high stresses at the joints between the arms which might affect the Q and to provide coupling between the arms so that they act as a single resonant structure and not as four independent arms.

To test the effect of the radius of curvature on the Q of the sensor and the coupling between the arms, three aluminum cruciforms were constructed which had the same dimensions with the exception of the radius of curvature at the center. (See Fig. 5). These sensors were also made larger (8 to 12 in.) than the earlier sensors in order to become familiar with the behavior of large, low frequency devices.

Cruciform No. 4 (Fig. 5(a)) had a radius of curvature of 2 in. with an over-all diameter of 12.3 in. Cruciform No. 5 (Fig. 5(b)) had a radius of curvature of 1 in. and a diameter of 10.3 in. Cruciform No. 6 (Fig. 5(c)) had a radius of only 0.25 in. and an over-all diameter of 8.8 in. Despite the large variation in size, they all had the same resonant frequency since the arm length (measured from the fillet boundary) was kept constant.

Barium titanate strain transducers were attached to the arms and the cruciforms were suspended at the center of mass by a small wire and a rubber strip to give minimum external coupling. By driving the various modes with an external ac voltage the results shown in Table III were obtained.

TABLE III

Mode Frequencies for Large Cruciforms

Sensor	Tuning Fork Mode cps	Translational Mode cps	Torsional Mode cps
Cruciform No. 4 (2 in. radius)	20.2	25.2	511
Cruciform No. 5 (1 in. radius)	20.1	26.5	930
Cruciform No. 6 (1/4 in. radius)	20.8	28.5	1698

There seemed to be no significant difference in the Q of the various units.

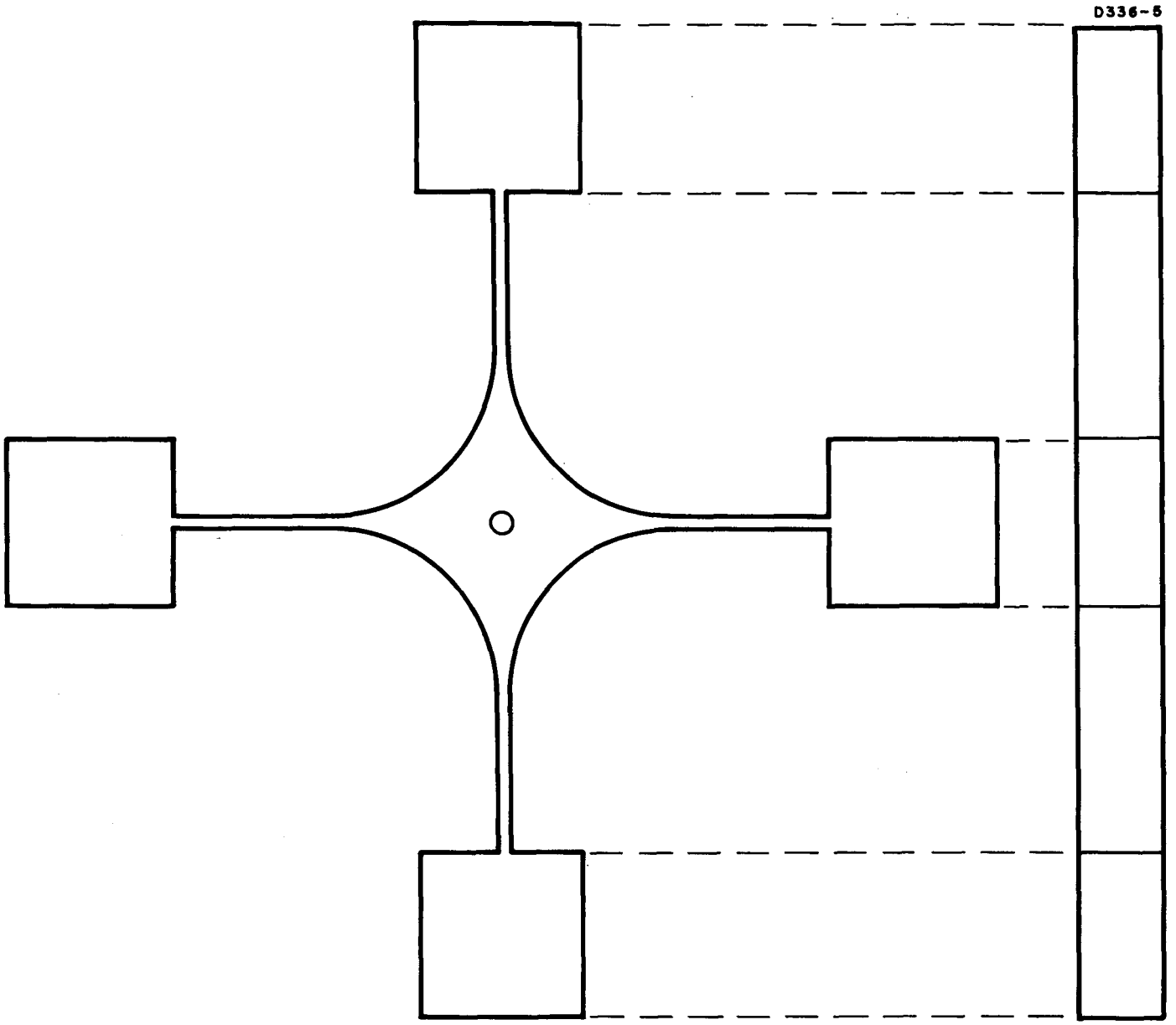

Fig. 5(a). Sensor cruciform (2 in. radius).

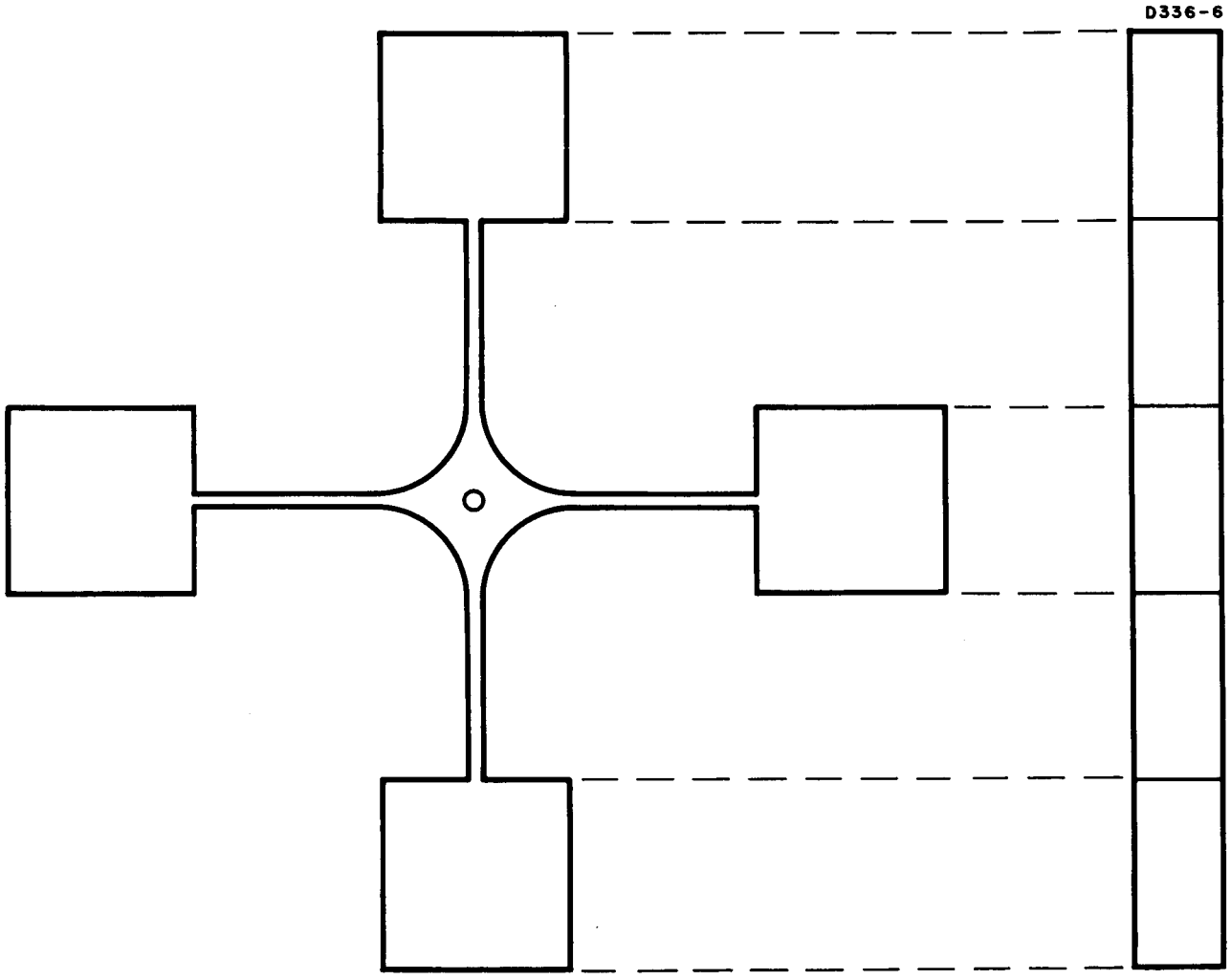

Fig. 5(b). Sensor cruciform (1 in. radius).

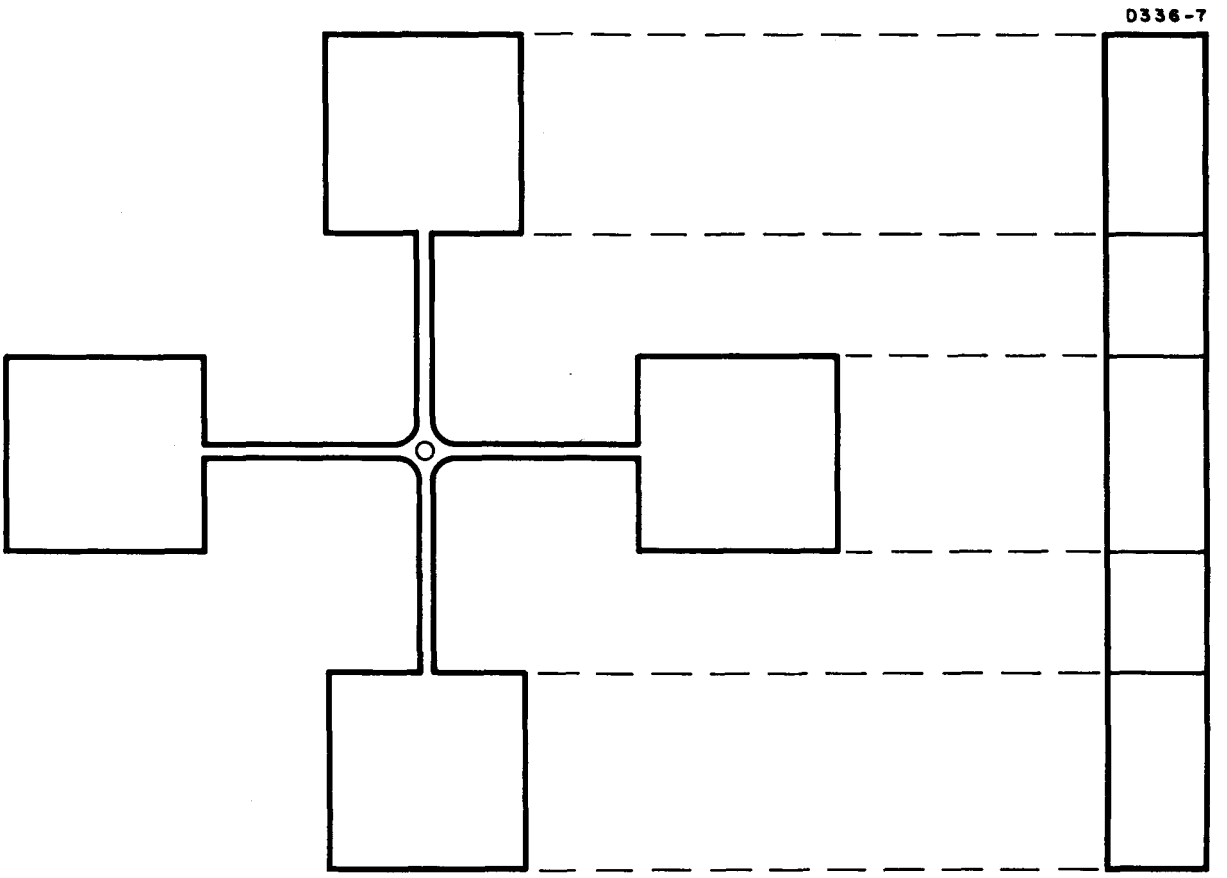

Fig. 5(c). Sensor cruciform (1/4 in. radius).

The major effect on the Q was found to be a result of damping from the barium titanate strain transducers on the arms. With two large (SC-4) tranducers, the Q of cruciform No. 6 was 160, with one large transducer it was 235, and with one small (SC-1) transducer the Q rose to 435.

Various tests were also run in air and in vacuum with the other conditions held constant. There was no apparent difference in Q or in the resonant frequency. The only effect noted was the lack of acoustical noise excitation in the vacuum.

The conclusions drawn from the above tests were that the primary cause of damping in the present sensors are the losses in the strain transducers and that the sensor with the smallest radius of curvature had the greatest frequency separation between the various vibrational modes because of its smaller center mass. Since the smaller radius does not seem to affect the other properties of the sensor, future sensor designs could have smaller radii of curvature than the designs shown in Quarterly Progress Report No. 1.

C. Air Bearing Support and Drive

An air bearing support and drive was constructed for us by the Hughes Aerospace Group in Culver City. The support structure consisted of a table supported both vertically and horizontally by an air bearing formed with a rotor tube sitting on a channeled stator. The rotor tube also has a magnetic hysteresis ring which is excited and driven by a synchronous motor stator constructed around the outside. (See Figs. 6 and 7 of this report and Fig. 11 of the first quarterly.) The sensor chamber is then mounted on top of the rotor table and the voltages from the sensor are removed through the slip rings on the top. The primary reason for the construction of this support and drive unit was to discover and investigate sources of vibrational noise in air bearings.

The synchronous motor drive worked very well, had a great deal of torque, could be run up to speed rapidly and was not difficult to synchronize. The air bearing had very low friction, as was to be expected; however, during the operational checks, two instabilities were discovered. One was a lateral dynamic resonance whose frequency varied with air pressure and the other was a vertical instability which was inaudible at low operating pressures, but which could be heard at pressures above 40 psi.

The lateral resonance would occur at speeds just short of the desired rotational speeds when the rotor table was loaded with the sensor chamber. However, by adjusting the pressure while running

M 3821

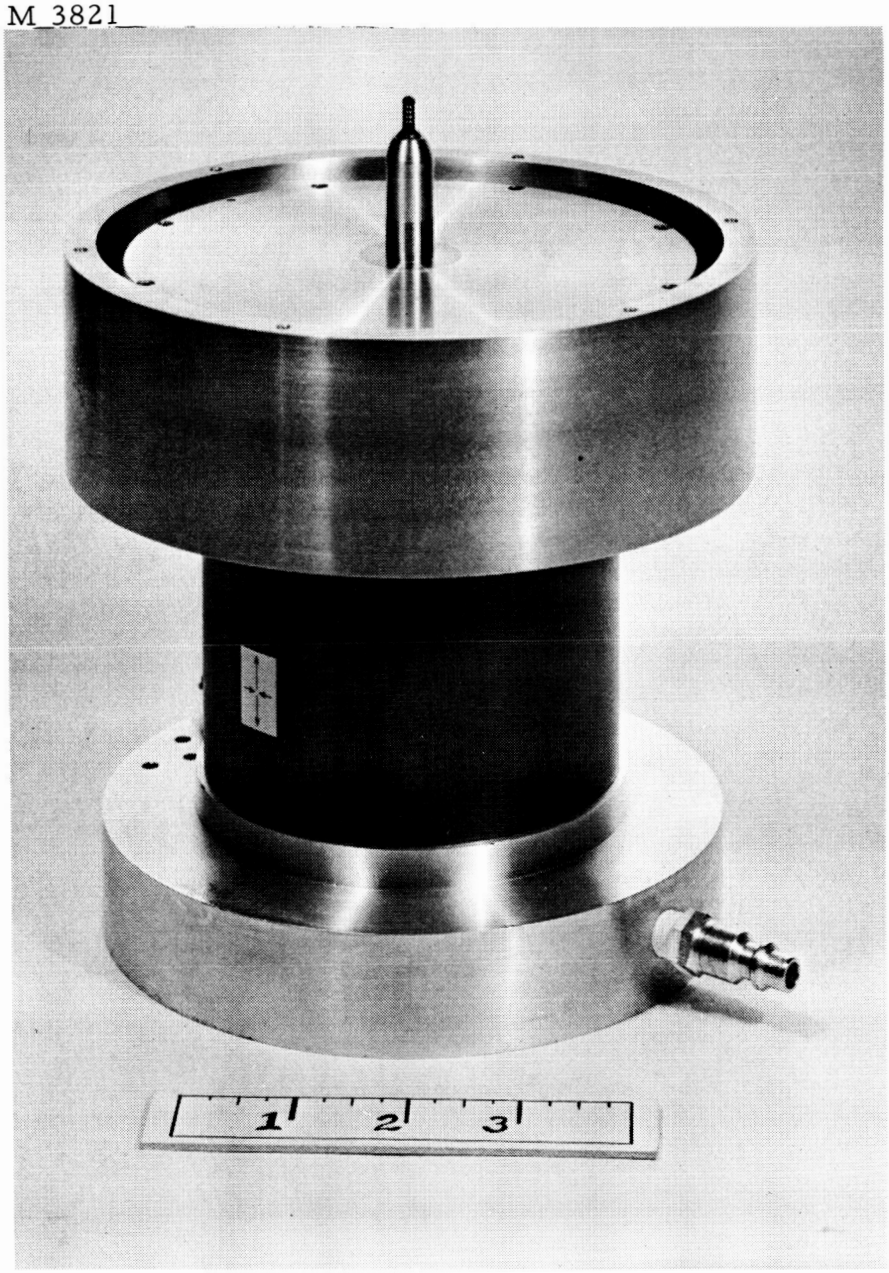

Fig. 6. Air bearing support and drive (assembled).

M 3822

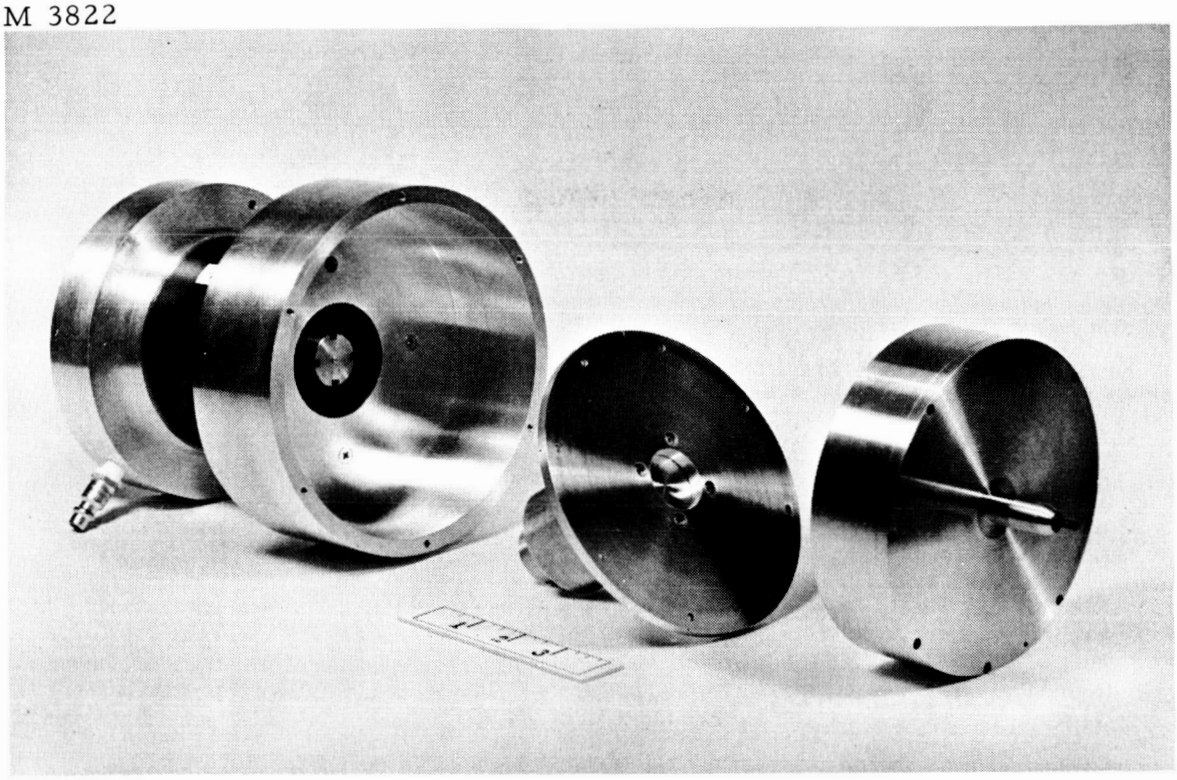

Fig. 7. Air bearing support and drive (exploded view).

up to speed it was found to be possible to pass through this resonance without damage to the rotor. If the sensor had been designed to work at a lower frequency (100 cps instead of 200 cps), this lateral resonance would not have been a problem.

The vertical instability, however, was a more serious problem. It occurred at all speeds, was nearly independent of the speed of rotation, and would even occur with a stationary, but levitated, table. The noise level introduced into the sensor by these vibrations was large enough to cause a sensor output in the millivolt range. A theoretical analysis (Section III-A) indicated the possible causes of this instability and the air bearing portion of the unit has been modified in an attempt to eliminate the problem. The radial gap has been lowered and the bearing pad itself has been changed. These modifications will be tested and reported during the next report period.

III. THEORETICAL PROGRAM

A. Air Bearing Analysis

Because of the vertical vibrations that were found in the air bearing which was constructed for us, it was decided to analyze the behavior of this type of system to determine the changes that would be necessary to eliminate this source of high frequency noise.

In order to make the analysis tractable, the simplified structure shown in Fig. 8 was used as the model and the following assumptions were made.

1. All expansion processes were isothermal
2. There is no pressure drop across the spotface area (point 1)
3. All frictional losses are negligible.

From conservation of momentum applied to expanding gases the pressure-velocity relationship in the tube at point 1 is

$$\frac{v_1^2}{2} = \frac{P_2}{\rho_2} \ln \frac{P_o}{P_1} \tag{17}$$

and the pressure-velocity relationship in gap g is

$$\frac{v^2}{2} - \frac{v_1^2}{2} = \frac{P_2}{\rho_2} \ln \frac{P_1 r_1}{Pr} \quad . \tag{18}$$

The equation for the conservation of mass ratio of flow in the gap is

$$\rho A v = \rho_1 A_1 v_1 \tag{19}$$

where A is the cross-sectional area of the air path or

$$v = v_1 \frac{\rho_1}{\rho} \frac{r_1}{r} \quad . \tag{20}$$

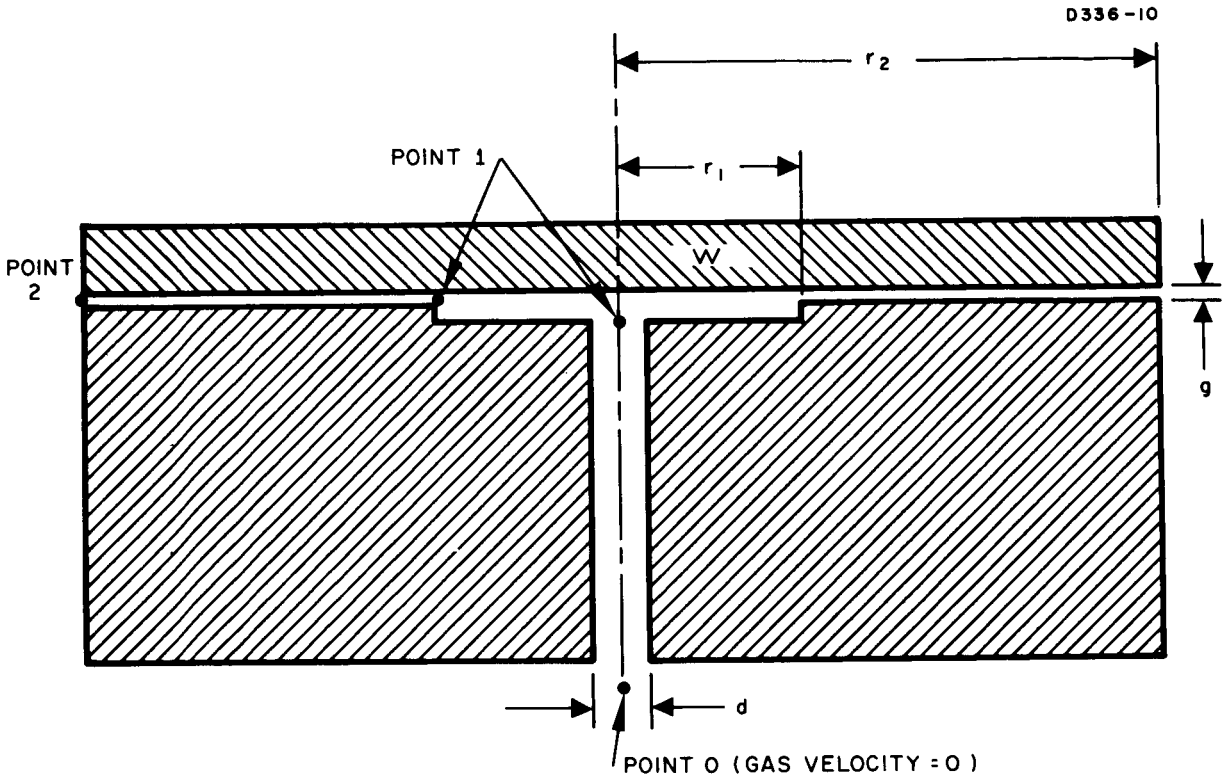

Fig. 8. Air bearing table schematic.

If we combine (17), (18), and (20) using the gas law for isothermal expansion that

$$\frac{P}{\rho} \equiv \text{constant} = \frac{P_2}{\rho_2} \quad , \tag{21}$$

we obtain

$$\left(\frac{P_1 r_1}{Pr}\right)^2 \ln \frac{P_o}{P_1} = \ln \frac{P_o r_1}{Pr} \tag{22}$$

or

$$P_1^2 \ln \frac{P_o}{P_1} = P^2 \left(\frac{r}{r_1}\right)^2 \ln \frac{P_o r_1}{Pr} \quad . \tag{23}$$

If we use the known atmospheric conditions at point 2

$$P_1^2 \ln \frac{P_o}{P_1} = P_2^2 \left(\frac{r_2}{r_1}\right)^2 \ln \frac{P_o r_1}{P_2 r_2} \tag{24}$$

to solve for P_1, we observe that this equation is satisfied by two values of P_1 for each value of P_o except where

$$\frac{d}{dP_1} \left[P_1^2 \ln \frac{P_o}{P_1}\right] = 0 \quad . \tag{25}$$

In performing this differentiation we find

$$2 \ln \frac{P_o}{P_1} = 1 \tag{26}$$

or

$$\frac{P_o}{P_1} = 1.65 \quad . \tag{27}$$

If we substitute this value into (22) we obtain

$$\left(\frac{P_1 r_1}{Pr}\right)^2 = 2 \ln \frac{P_1 r_1}{Pr} + 1 \tag{28}$$

or

$$\left(\frac{P_1 r_1}{Pr}\right)^2 - 2 \ln \frac{P_1 r_1}{Pr} = 1 \quad . \tag{29}$$

However, this is only true when

$$Pr = P_1 r_1 \quad . \tag{30}$$

Therefore, in gap g the product Pr is constant and

$$P_1 r_1 = Pr = P_2 r_2 \quad , \tag{31}$$

or (using (27)),

$$\frac{r_1}{r_2} = \frac{1.65 P_2}{P_o} \quad . \tag{32}$$

The following summarizes the above portion of the analysis.

In order to obtain a truly stable air bearing support the pressures across the support pads should be constant and single valued. If the system is subjected to external pressures of P_o and P_2 the internal pressure is made single valued by giving the ratio r_1/r_2 the value provided by (32). Note also that (from (18) and (31))

$$\frac{v^2}{2} - \frac{v_1^2}{2} = 0 \quad ,$$

or the air velocity anywhere in the gap is constant. In order to determine the actual value of P_o required, we equate the upward force produced by the air pressure in the gap to the weight supported by the pad.

$$F = \pi r_1^2 P_1 + \int_1^2 2\pi r P dr - \pi r_2^2 P_2 \tag{33}$$

$$F = 2\pi \int_1^2 P r dr + \pi(P_1 r_1^2 - P_2 r_2^2) \quad . \tag{34}$$

However, from (31) we know that

$$Pr = P_2 r_2 \; ; \tag{31}$$

therefore,

$$F = 2\pi P_2 r_2 [r_2 - r_1] + \pi P_2 r_2 [r_1 - r_2] \; , \tag{35}$$

and, by combining terms,

$$F = \pi P_2 r_2^2 \left[1 - \frac{r_1}{r_2}\right] . \tag{36}$$

However, from (32) we know that

$$\frac{r_1}{r_2} = \frac{1.65\, P_2}{P_o} \; ; \tag{32}$$

therefore,

$$F = \pi P_2 r_2^2 \left[1 - \frac{1.65\, P_2}{P_o}\right] = W \tag{37}$$

or, the desired operating pressure is

$$P_o = \frac{1.65\, \pi P_2^2 r_2^2}{\pi P_2 r_2^2 - W} \quad . \tag{38}$$

In calculating for the sensor design we use (32) and (38) and environmental conditions as follows:

$$W = 4.74 \text{ lb}$$

$$r_2 = 0.375 \text{ in.}$$

$$P_2 = 14.7 \text{ psia} \quad .$$

We can solve for P_o and r_1

$$P_o = 90 \text{ psia} \tag{39}$$

$$r_1 = 1.65 \frac{P_2}{P_o} r_2$$

$$= 0.101 \text{ in.} \tag{40}$$

A new spud, or air bearing stator, was constructed with different dimensions based on the above analysis; this spud will be investigated in the future.

B. Cruciform Sensor Analysis

Since we have found by experiment that a transversely vibrating cruciform structure can be rotated at the speeds necessary for interaction with gravitational force gradients, it appears that this type of sensor configuration should be used in our first models. A detailed analysis of these sensors was started in order to develop a more complete understanding of their behavior; this will enable us to interpret their operation on the earth, predict their operation in free fall, and optimize their structure parameters.

The model used for the analysis is shown in Fig. 9. It consists of a central mass M_6, four equal sensor masses M_1 - M_4, and a sensed mass M_5. The force on the ith mass is then given by

$$F_i = \frac{GM_iM_5}{R_i^2} \tag{41}$$

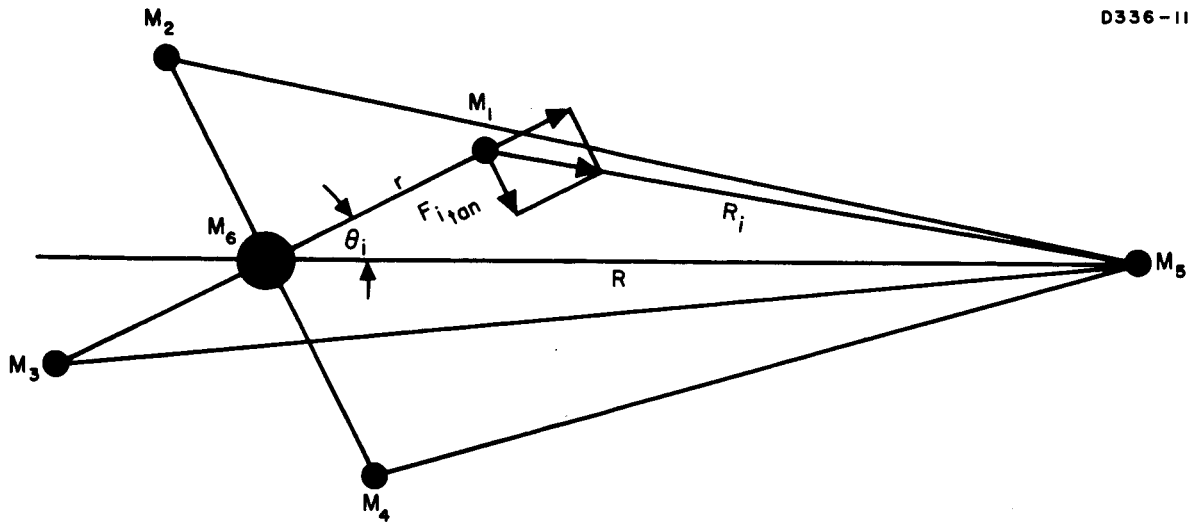

Fig. 9. Cruciform analysis schematic.

and the tangential component of this force is

$$F_{i_{tan}} = \frac{GM_iM_5 \; R \sin \theta_i}{R_i^3} \quad . \tag{42}$$

However,

$$R_i^2 = R^2 + r^2 - 2Rr \cos \theta_i \tag{43}$$

and therefore

$$F_{i_{tan}} = \frac{GM_iM_5}{R^2} \; \frac{\sin \theta_i}{\left[1 + \left(\frac{r}{R}\right)^2 - 2\left(\frac{r}{R}\right) \cos \theta_i\right]^{3/2}} \quad . \tag{44}$$

If we expand the denominator and combine terms in the same frequency, we obtain the equation of motion

$$F_{i_{tan}} = \frac{GM_5M_i}{R^2} \left[\sin \theta_i + \frac{3}{2} \frac{r}{R} \sin 2\,\theta_i + \frac{15}{8} \left(\frac{r}{R}\right)^2 \sin 3\,\theta_i + \frac{35}{16} \left(\frac{r}{R}\right)^3 \sin 4\,\theta_i\right] \tag{45}$$

where

$$\theta_i = \theta_{oi} + \omega t + \phi_i \cong \theta_{oi} + \omega t \quad ,$$

$$\theta_{oi} = (i - 1) \frac{\pi}{2}$$

and ϕ_i is the vibration angle from the reference on mass 6. If we assume no interactions through the hub and that $\theta_i = \omega t$ we can solve the equation of motion (45) for M_i with the result

$$\Phi_i = \frac{GM_5M_i}{rR^2}\left[\frac{\sin(\omega t - \gamma_i)}{\sqrt{(K - m\omega^2)^2 + (D\omega)^2}} + \frac{3}{2}\frac{r}{R}\frac{\sin(2\omega t - \gamma_2)}{\sqrt{(K - 4m\omega^2)^2 + (2D\omega)^2}}\right.$$

$$+ \frac{15}{8}\left(\frac{r}{R}\right)^2 \frac{\sin(3\omega t - \gamma_3)}{\sqrt{(K - 9m\omega^2)^2 + (3D\omega)^2}}$$

$$\left. + \frac{35}{16}\left(\frac{r}{R}\right)^3 \frac{\sin(4\omega t - \gamma_4)}{\sqrt{(K - 16m\omega^2)^2 + (4D\omega)^2}}\right] \tag{46}$$

where

$$\gamma_i = \tan^{-1}\frac{D\omega}{K - m(i\omega)^2} \quad . \tag{47}$$

If the arms are tuned to a resonant frequency of 2ω, $(K/M_i = 4\omega^2)$, then the steady state 2ω amplitude is

$$\phi_{2\omega} = \frac{3}{2}\frac{GM_5M_i}{R^3}\left[\frac{1}{2D\omega}\right] \tag{48}$$

but

$$D = \frac{2\omega M_i}{Q} \tag{49}$$

$$\therefore \phi_{2\omega} = \frac{3}{8}\frac{GM_5Q}{R^3\omega^2} \quad . \tag{50}$$

Since we are using strain transducers to detect the deflection of the arms, we must relate the voltage out of the transducers V_{out} to the deflection ϕ using the theory of bent beams. The voltage out is directly proportional to the strain, and the strain ϵ in the beam is proportional to the deflection angle for small deflections.

$$V_{out} = \sigma\epsilon = \sigma \frac{hr}{L^2} \phi \tag{51}$$

where

$\sigma \equiv$ transducer factor ($\sim 10^5$ volts/in./in. for barium titanate units)

$r \equiv$ radial distance of sensor end mass from center of sensor rotation

$L \equiv$ length of sensor arms

$h \equiv$ thickness of sensor arms.

Combining (51) and (50), the maximum voltage out of the sensor due to the gravitational gradient of the mass M_5 is

$$V_{out} = \frac{3GM_5}{8R^3} \frac{\tau}{\omega} \frac{hr}{L^2} \sigma \sin 2\omega t \tag{52}$$

where

$GM_5/R^3 \equiv$ gravitational gradient

$\omega \equiv$ angular frequency of rotation of sensor

$\tau \equiv$ integration time.

The output for the cruciform sensor predicted by the above equation is lower by a factor of hr/L^2 than the output of a similar sized radial spring sensor. In the original designs this factor is about 0.07. Other sensor designs which will increase the voltage output by varying the parameters h, r, and L are being considered.

The above simplified solution is adequate for an order of magnitude estimate of the output of the sensor, but it neglects the interaction of the arms through the stresses in the hub, the effect of relative rotation of the hub and outer masses, and assumes constant angular rotation rather than constant angular momentum. A more detailed analysis which takes these factors into account and which also allows for the calculation of the effect of slight mass imbalances or arm length differences is under way. The calculations result in a complex set of coupled equations which require solution on an analog computer. This work will be reported in the next quarterly progress report.

IV. CONCLUSIONS

The cruciform structure is usable as a sensor head in prototype gravitational mass sensor studies since its gradient sensing vibrational mode can be separated from the other modes of vibration. In addition, the structure is capable of being rotated at the necessary speeds. However, further work needs to be done on optimizing the sensor parameters and developing sensor mounting structures.

Air bearings have a number of vibrational noise sources which require further investigation.

The available electronic techniques for sensing the vibrational strains, amplifying the signals, and bringing them out from the rotor are more than adequate for the problem.

The major problem area is still that of bearing noise.

V. RECOMMENDATIONS

It is recommended that the following investigations be continued:

1. Experimental investigation of noise in bearings and drives

2. Experimental investigation of sensor mounts

3. Preliminary studies of other sensor structures

4. Theoretical analysis of the cruciform sensor.

It is further recommended that sometime before 31 July 1965 the results of the program to date be reviewed with the contracting officer and the general design of the feasibility model and the work outline for the second phase of the contract be approved.